The local and intermediate range structures of the five amorphous ices at 80 K and ambient pressure: A Faber-Ziman and Bhatia-Thornton analysis

D. T. Bowron[a)]
ISIS Facility, Rutherford Appleton Laboratory, Chilton, Didcot, Oxon, OX11 0QX, United Kingdom and Department of Physics and Astronomy, University College London, Gower Street, London WC1E 6BT, United Kingdom

J. L. Finney
Department of Physics and Astronomy, University College London, Gower Street, London WC1E 6BT, United Kingdom

A. Hallbrucker, I. Kohl, T. Loerting, and E. Mayer
Institute of General, Inorganic and Theoretical Chemistry, University of Innsbruck, A-6020 Innsbruck, Austria

A. K. Soper
ISIS Facility, Rutherford Appleton Laboratory, Chilton, Didcot, Oxon, OX11 0QX, United Kingdom and Department of Physics and Astronomy, University College London, Gower Street, London WC1E 6BT, United Kingdom

Using isotope substitution neutron scattering data, we present a detailed structural analysis of the short and intermediate range structures of the five known forms of amorphous ice. Two of the lower density forms—amorphous solid water and hyperquenched glassy water—have a structure very similar to each other and to low density amorphous ice, a structure which closely resembles a disordered, tetrahedrally coordinated, fully hydrogen bonded network. High density and very high density amorphous ices retain this tetrahedral organization at short range, but show significant differences beyond about 3.1 Å from a typical water oxygen. The first diffraction peak in all structures is seen to be solely a function of the intermolecular organization. The short range connectivity in the two higher density forms is more homogeneous, while the hydrogen site disorder in these forms is greater. The low Q behavior of the structure factors indicates no significant density or concentration fluctuations over the length scale probed. We conclude that these three latter forms of ice are structurally distinct. Finally, the x-ray structure factors for all five amorphous systems are calculated for comparison with other studies. © *2006 American Institute of Physics*.
[DOI: 10.1063/1.2378921]

I. INTRODUCTION

It is generally recognized that there are five different kinds of amorphous ice, distinguished originally by their methods of preparation. The first, amorphous solid water (ASW), was produced by depositing water vapor on a cold substrate, first by Burton and Oliver in 1935.[1] Later work has demonstrated that it can be consistently formed by deposition at liquid nitrogen temperature.[2] As formed, this material is microporous:[3] it can be consolidated by annealing or sintering at a high temperature below about 120 K. Another noncrystalline form, hyperquenched glassy water (HGW), can be prepared by very rapid cooling of liquid droplets by either injecting a fine water spray into a cryoliquid or supersonically impacting micron-sized droplets onto a substrate at 77 K.[4,5] Pressurizing crystalline ice Ih to about 1 GPa at 77 K results in another apparently amorphous phase.[6] This was labeled high density amorphous ice (HDA) on account of its significantly higher density. Controlled heating of HDA recovered to ambient pressure produced a "low density

amorph" (LDA) above about 120 K.[7] A very high density form (VHDA) was discovered very recently by isobaric heating of HDA under pressure.[8]

Using isotope substitution neutron diffraction techniques, the short range atomic level structures of LDA, HDA, and VHDA have been reported briefly.[9,10] Despite a significant amount of experimental work, the detailed structures of the two earlier-discovered forms, ASW and HGW, have not been definitively solved. Although there is an expectation that their atomic level structures are similar to that of LDA, earlier experimental work, including calorimetry and spectroscopy, has not fully supported this hypothesis. Neutron total diffraction patterns of ASW and HGW show similarities, but the published patterns are not sufficiently identical to confirm structural identity, nor to demonstrate identity with LDA.[11–13] Other work has also produced diffraction patterns for ASW and HGW that differ from each other in varying degrees, and from that of LDA.[14–16]

We present here the results of neutron diffraction isotope substitution experiments on all five forms of amorphous ice at 80 K and ambient pressure. The earlier reported data on

a)Electronic mail: d.t.bowron@rl.ac.uk

LDA, HDA, and VHDA have been reanalyzed using improved software.[17] In the previous analysis[9,10] the experimental differential cross-section data were inverted directly to site-site partial structure factors, and then analyzed using a three dimensional atomistic model. In the present analysis the differential cross-section data are modeled directly, which helps eliminate artifacts that might arise from systematic errors in the data.[17] In fact, in the present instance the results of the new analysis are closely similar to the previous reported structures. Both the Faber-Ziman and Bhatia-Thornton partial structure factors and partial radial distribution functions are presented. These are discussed in terms of both the short and intermolecular range structures of all five amorphous forms. The structural similarity of ASW, HGW, and LDA is quantitatively confirmed. Expected x-ray structure factors are also presented. Finally, an attempt to reproduce the structure of HDA as a mixture of the higher and lower density forms VHDA and LDA leads us to conclude that, on length scales up to about 10 Å, HDA is a distinct structural form.

II. THEORY

After normalization to a standard scattering sample, vanadium, and following corrections for background scattering, sample absorption, multiple scattering, inelastic scattering, and atomic self-scattering, the function measured in a neutron diffraction experiment is the interference differential scattering cross section, $F(Q)$, see, e.g., Ref. 18. Q is defined as the magnitude of the momentum transfer vector of the scattering process:

$$Q = \frac{4\pi}{\lambda} \sin \theta. \tag{1}$$

The wavelength of the incident neutrons is λ and 2θ is the scattering angle. In terms of this variable, $F(Q)$ can then be written as

$$F(Q) = \sum_{\alpha \leqslant \beta} (2 - \delta_{\alpha\beta}) c_\alpha c_\beta b_\alpha b_\beta (S_{\alpha\beta}(Q) - 1). \tag{2}$$

This function includes information relating to the pairwise spatial correlations between atoms of types α and β, which is contained in the sum over the site-site, or Faber-Ziman, partial structure factors, $S_{\alpha\beta}(Q)$. These in turn are weighted by the respective concentrations, c_α and c_β, and scattering lengths, b_α and b_β, of each atom type. To avoid double counting of the like terms within the summation, $\delta_{\alpha\beta}$ is the Kronecker delta function. A particular advantage of the neutron scattering method is that this interference function is measured on an absolute scale in units of b/sr/atom and is calibrated against the scattering from the known level of the vanadium standard. The absolute nature of the measurement thus allows the chemical and isotopic composition of the sample to be checked if the density of the sample is known.

The structure factors, either composite or partial, can be inverted to real space atomic pair distribution functions, $g_{\alpha\beta}(r)$, by a Fourier transform weighted by the atomic density ρ:

$$(g_{\alpha\beta}(r) - 1) = \frac{1}{2\pi^2\rho} \int_0^\infty Q^2 (S_{\alpha\beta}(Q) - 1) \frac{\sin Qr}{Qr} dQ. \tag{3}$$

$g_{\alpha\beta}(r)$ is the interatomic pair distribution function containing information about the number of atoms of type β about atoms of type α, or vice versa, as a function of their separation r.

If a single neutron scattering experiment is performed, it is only possible to measure the total interference differential scattering cross section, as knowledge of the concentrations and neutron scattering lengths of the component atoms is insufficient to allow the separation of $F(Q)$ into the individual partial structure factors, $S_{\alpha\beta}(Q)$. However, if a sample contains elements where isotopes of different neutron scattering lengths are available, it becomes possible to perform a series of measurements to circumvent this difficulty.[19] Each measurement is performed on a sample that has the same chemical composition as the others but differing isotopic composition. Under the assumption that each of these isotopic analogs is structurally identical, it is then possible to extract the partial structure factors for the system, provided that a sufficient number of isotope contrasts are available, and hence obtain specific pairwise atomic correlations. Such an extraction is possible in this case because H and D have markedly different scattering lengths[20] so that a suitable set of isotopically distinct samples can be prepared.

III. EXPERIMENT

Samples of VHDA,[8,9] HDA,[10] ASW,[21] and HGW (Ref. 22) were prepared from H_2O, D_2O, and a 50:50 mixture of H_2O and D_2O. The structural consistency of these isotopic samples was checked with x-ray diffraction following their production. The preparation methods can be summarized as follows.

(1) VHDA was prepared in a piston cylinder press via the formation of HDA by (i) the compression of ice Ih at 77 K to a pressure of 1.5 GPa, followed by (ii) annealing the structure at a pressure of 1.1 GPa and a temperature of 165 K, and finally (iii) quenching the sample to a temperature of 77 K to facilitate recovery at ambient pressure. The isotopic compositions of the D_2O and HDO samples were determined by IR spectroscopy to be 99.0% and 49.7% D, respectively.

(2) HDA was similarly prepared in a piston cylinder press by compression of ice Ih at 77 K to a pressure of 1.6 GPa, and again recovered under liquid nitrogen at ambient pressure. As with the VHDA sample IR spectroscopy was used to determine the isotopic compositions of the D_2O and HDO samples to be 99.9% and 49.6% D, respectively.

(3) Samples of ASW were prepared by deposition of water vapor for 10–12 h onto a substrate precooled to 77 K. Water vapor pressure at the source during deposition was 0.10 mbar. After deposition, ASW samples were heated *in vacuo* up to ≈ 120 K in order to close the micropores and reduce the apparent surface area of the deposit by "sintering."[3] The isotopic compositions of the D_2O and HDO samples were found by IR spectros-

copy to be 99.9% and 49.7% D, respectively.

(4)   HGW samples were prepared as in Ref. 22. An ultrasonic nebulizer operating at 3 MHz (LKB Instruments, model 108) was used to generate droplets of ≈ 3 μm diameter. The aerosol was transferred with nitrogen (purity of 99.995%) as carrier gas through a silicon tube (1 m long, 20 mm inner diameter) which is cooled with ice water in order to reduce the relative amount of water vapor. Thereafter, it was conveyed through an electron microscopic aperture of 300 μm diameter, into the high vacuum system. Deposition time varied between 20 and 24 min, and the thickness of the hyperquenched deposit was between ≈ 1 and 2 mm. IR spectroscopy established the isotopic compositions of the D_2O and HDO samples to be 97.2% and 49.8% D, respectively.

The samples of LDA were prepared *in situ* during the neutron scattering experiments by controlled heating of the HDA samples to 122 K and recooling to 80 K for the structural measurements.[8] As these samples were formed directly from the HDA samples, the isotopic compositions of the D_2O and HDO systems were accordingly 99.9% and 49.6% D, respectively.

The atomic densities of the VHDA,[8] HDA,[7] and LDA (Ref. 7) samples were determined by buoyancy using a liquid cryogen and found to be 0.125, 0.117, and 0.094 atoms/Å^3, respectively. The densities of the ASW and HGW samples were taken to be the same as that of the LDA system.[23]

For the measurement of their neutron diffraction patterns each sample of VHDA, HDA, ASW, and HGW was powdered with a pestle and mortar and loaded into parallel sided "null scattering" TiZr alloy cells of internal dimensions of $35 \times 35 \times 2$ mm^3 and wall thickness of 1.1 mm. All sample handling and loading procedures were performed under liquid nitrogen and the samples were immediately transferred into a cryostat held at 80 K for measurement and any residual liquid nitrogen transferred with the sample pumped out of the sample volume.

The scattering data were collected on the Small Angle Neutron Diffractometer for Amorphous and Liquid Samples (SANDALS) at the ISIS pulsed neutron facility, Oxfordshire, U.K. The data were measured over scattering angles (2θ) between 3° and 40° and analyzed using neutron wavelengths in the range from $\lambda = 0.05$ to 1.5 Å over a corresponding Q range for each data set ranging from 0.5 to 30 Å^{-1}. After collection the data were reduced to the interference differential scattering cross section using the GUDRUN routines[24] that are based upon basic algorithms in the widely used ATLAS package.[25] These routines correct the data for the contributions from the empty cell, empty cryostat, instrument background, absorption, and multiple scattering and normalize the data to absolute units using the scattering of a vanadium standard. The remaining corrections to account for the contributions from inelastic scattering by the sample were made using the methods outlined in Soper and Luzar.[26]

A challenge for the normalization of scattering data from powdered samples is correction for the imperfect packing of
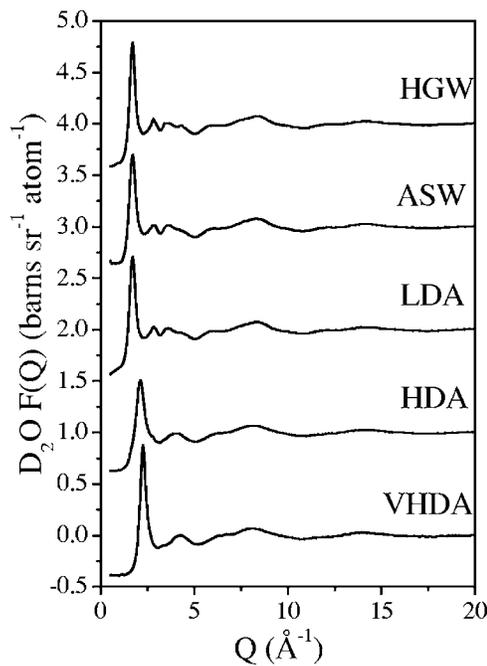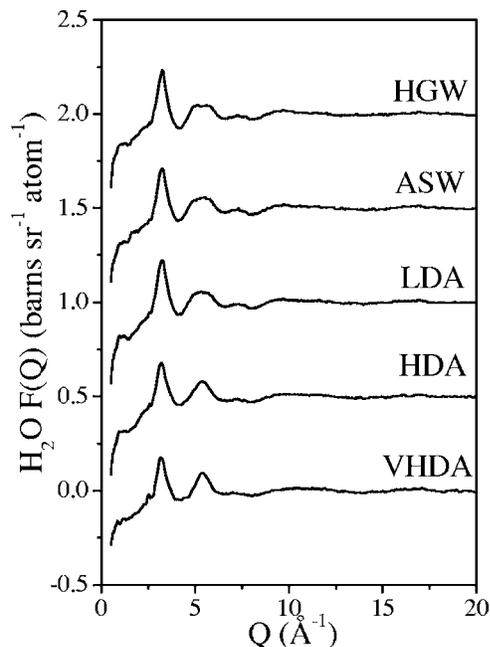

FIG. 1. The fully corrected experimentally measured interference differential scattering cross sections $F(Q)$ for VHDA, HDA, LDA, ASW, and HGW ices prepared using D_2O. For clarity the functions are vertically offset by 0, 1.0, 2.0, 3.0, and 4.0 units, respectively.

the sample. A particular advantage of the time-of-flight neutron scattering technique in the SANDALS flat plate sample geometry is that, after normalization of the raw data to the vanadium scattering and corrections for background, multiple scattering, and attenuation, but before correction for self-scattering, the measured total differential scattering intensity oscillates about a level (the high Q limit), given by

$$\lim_{Q \to \infty} I(Q) = \frac{\rho t f \sum_i c_i \sigma_i}{4\pi}, \tag{4}$$

where ρ is the sample density, t is the sample thickness, f is the packing fraction of the sample, c_i is the fraction of atoms of type i, and σ_i is the total scattering cross section of atoms of type i. Since the total scattering cross section is known from tables,[20] and the composition and density of each sample are known or measured, this high Q limit allows each measured data set to be scaled to compensate for packing effects. In the present instance the packing fraction varied between ~0.25 and ~0.6 with a precision of about 5%. This range reflects the variable success of packing individual samples into the cells under the handling challenges imposed by the need to maintain their immersion in liquid nitrogen at all times.

Figures 1–3 show the fully corrected interference differential scattering cross-section data for D_2O, H_2O, and HDO for each of the five amorphous ice samples investigated. It should be noted that there was no sign in any of the samples of significant small angle scattering down to the lowest Q value accessed (0.5 Å^{-1}). The lack of any small angle scattering in the data rules out the possible existence, in these samples, of mesoscale inhomogeneities on length scales of $\lesssim \approx 10$ Å. Of note is the absence of any evidence for re-
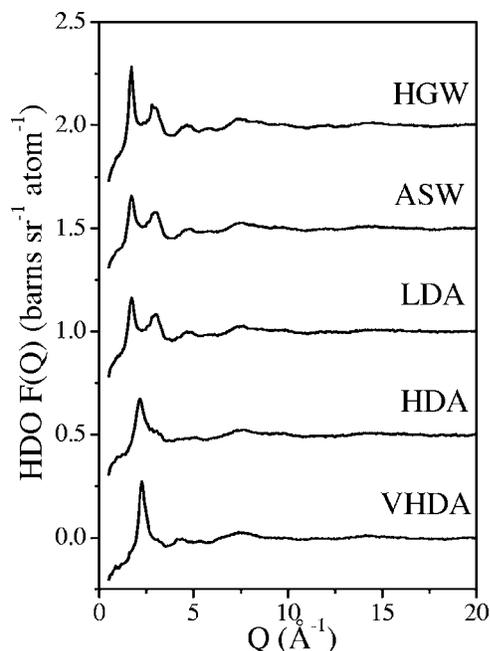
FIG. 2. The fully corrected experimentally measured interference differential scattering cross sections $F(Q)$ for VHDA, HDA, LDA, ASW, and HGW ices prepared using H_2O. For clarity the functions are vertically offset by 0, 0.5, 1.0, 1.5, and 2.0 units, respectively.

sidual crystallinity in any of the samples investigated here. Earlier studies of HGW (Ref. 22) have shown evidence for a small degree of residual crystallinity <5%, but this may reflect the difference between the structural probes. Neutrons are essentially a bulk probe due to their highly penetrating nature and are thus less sensitive to any surface effects that are often enhanced in x-ray studies.

FIG. 3. The fully corrected experimentally measured interference differential scattering cross sections $F(Q)$ for VHDA, HDA, LDA, ASW, and HGW ices prepared using a 50:50 mixture of H_2O and D_2O. For clarity the functions are vertically offset by 0, 0.5, 1.0, 1.5, and 2.0 units, respectively.

IV. STRUCTURE REFINEMENT

Detailed structural information was extracted through the construction of a three dimensional model that is constrained by the independent data sets. For the five amorphous ice systems studied here, the technique of empirical potential structure refinement (EPSR) has been employed.[17,27] This technique uses classical Monte Carlo simulation methods to build three dimensional structures that are as consistent as possible with the experimental data. The process is initiated by the equilibration of a structural model based purely on the known chemical stoichiometry and geometry of the molecular components, the atomic density of the system, and a series of pairwise potentials based on Lennard-Jones parameters and charges. Once the model is equilibrated, neutron diffraction patterns are calculated from the model, appropriately weighted for the isotopic composition of the experimentally measured samples, and the calculated differential scattering cross sections compared with the data. As the first model comparison is unlikely to reproduce the experimental data sufficiently well, a perturbation potential is then generated, based upon the difference function between the experimental data and the model. The simulation is then continued to allow the perturbation potential to evolve iteratively. Eventually a point is reached where the atomic and molecular configurations calculated from the model are an acceptable match to the experimental data. At this point the perturbation potential is considered to be adequately refined and the Monte Carlo modeling is continued under the sum of the reference plus perturbation potentials. Any desired structural information can then be extracted via ensemble averaging over many configurations of the molecules, all of which are consistent with the diffraction data as well as other known information such as the internal structure of the molecules themselves and the atomic density of the system.

This last point is significant when investigating glassy systems that by definition are not in a thermodynamic equilibrium state and their structure is sensitive to their thermodynamic history. This is a particularly important issue when considering isotopically distinct samples that are produced independently such as the H_2O, D_2O, and HDO systems investigated here. If a single structural model can be constructed that simultaneously satisfies the available experimental data, then one can conclude that within the sensitivity of the structural probe the samples are structurally analogous.

The simulations were initialized in cubic boxes containing 1800 water molecules and of side length of 35.1, 35.9, or 38.8 Å to be consistent with the known atomic density of the ice systems of 0.125, 0.117, or 0.094 atoms $Å^{-3}$, respectively. The configuration of individual molecular units within the simulation was periodically varied within harmonic constraints though maintaining the correct average molecular distances.[28] This process is a necessary addition to the standard Monte Carlo simulation method as the real experimental data reflect Debye-Waller broadening from quantum zero-point energy effects.

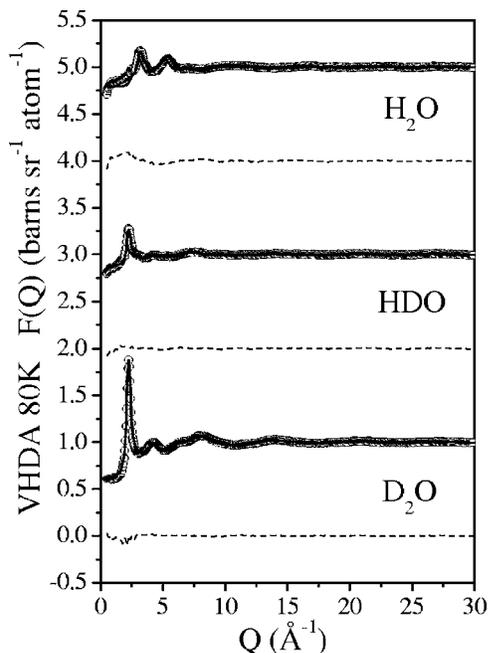Figures 4–6 show the EPSR fits and residuals for the VHDA, HDA, and LDA ice systems and demonstrate the
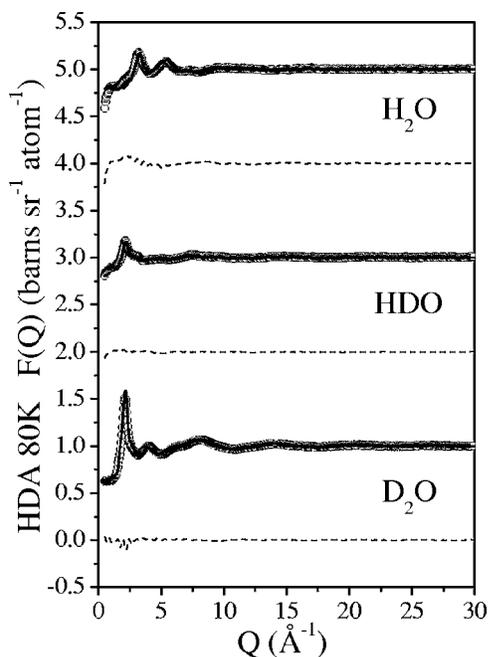
FIG. 4. The EPSR model fits (solid line) and fit residuals (broken line) to the D_2O, HDO, and H_2O experimental data (open circles) for VHDA. For clarity the model fits and experimental data are vertically offset by 1.0, 3.0, and 5.0 units, respectively, for the D_2O, HDO, and H_2O samples, while the corresponding fit residuals are vertically offset by 0.0, 2.0, and 4.0 units.

capability of the models to simultaneously satisfy the experimental data for each of the isotopically distinct systems on the same amorphous ice forms. The EPSR models for the ASW and HGW systems (not shown) are indistinguishable in quality from those of LDA.

FIG. 5. The EPSR model fits (solid line) and fit residuals (broken line) to the D_2O, HDO, and H_2O experimental data (open circles) for HDA. For clarity the model fits and experimental data are vertically offset by 1.0, 3.0, and 5.0 units, respectively, for the D_2O, HDO, and H_2O samples, while the corresponding fit residuals are vertically offset by 0.0, 2.0, and 4.0 units.
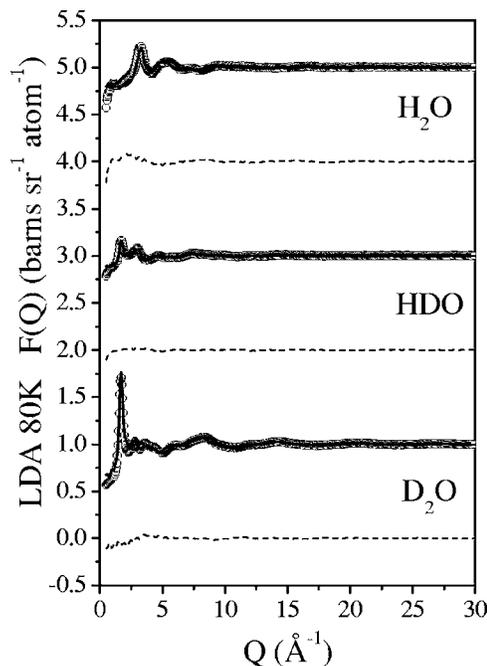
FIG. 6. The EPSR model fits (solid line) and fit residuals (broken line) to the D_2O, HDO, and H_2O experimental data (open circles) for LDA. For clarity the model fits and experimental data are vertically offset by 1.0, 3.0, and 5.0 units, respectively, for the D_2O, HDO, and H_2O samples, while the corresponding fit residuals are vertically offset by 0.0, 2.0, and 4.0 units.

V. RESULTS

In this study the following labels were assigned to the atomic sites on the water molecules: O and H for the water oxygen atom and two hydrogen atoms, respectively. The Lennard-Jones parameters, atomic masses, and fractional charges used to seed the modeling process taken from the widely used SPC/E parametrization of the water molecule are summarized in Table I (Ref. 29) with the assumed OH and HH intramolecular distances set to 0.976 and 1.55 Å, respectively.

A. Faber-Ziman partial structure factors and pair distribution functions

As the structure refinement procedure results in a three dimensional structural model that is consistent with the experimental data, it is a trivial procedure to extract experimentally consistent structural correlation or distribution functions. Arguably the most informative correlation functions are the Faber-Ziman partial structure factors that tell us about the pairwise interactions between atoms of specific type. In the amorphous ice system, three correlation functions are required to completely characterize the system. These are (i)

TABLE I. Lennard-Jones, charge, and atomic mass parameters used for the reference potentials that seed the empirical potential structure refinement model for the amorphous ices.

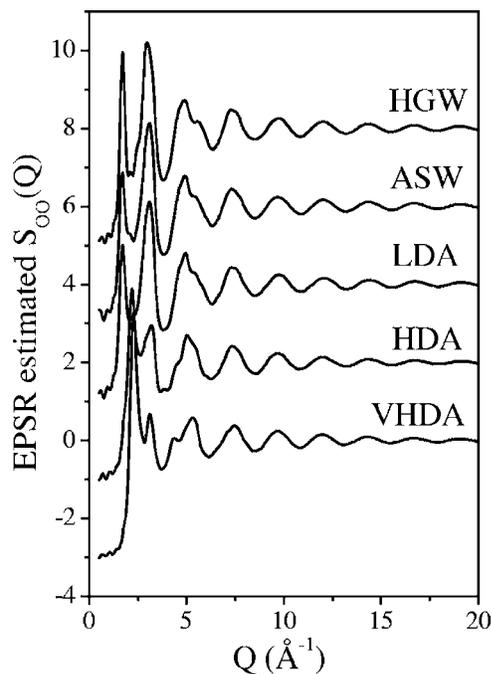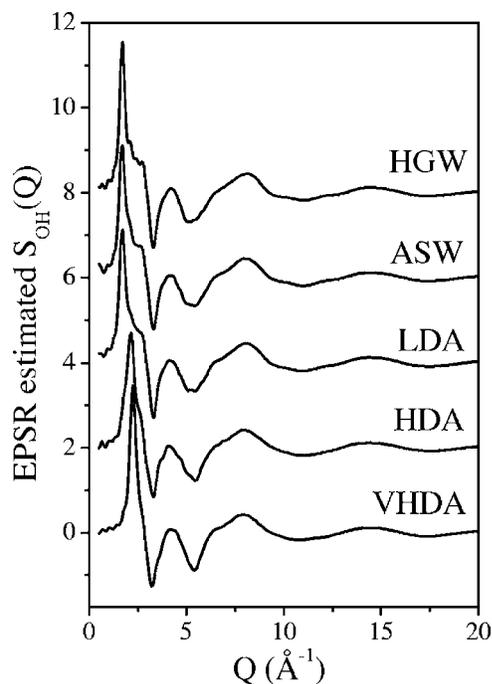| Atom type	ε (kJ mol^{-1})	σ (Å)	M (amu)	q (e)
O	0.650	3.17	16	−0.8476
H	0.000	0.00	2	0.4238

FIG. 7. The EPSR estimated oxygen-oxygen partial structure factors $[S_{OO}(Q)-1]$ for VHDA, HDA, LDA, ASW, and HGW that are consistent with the measured experimental data. For clarity each function is vertically offset by 0.0, 2.0, 4.0, 6.0, and 8.0 units, respectively.
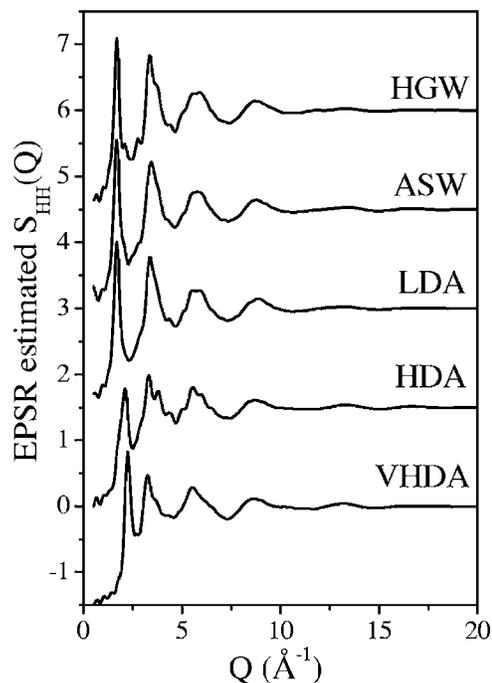

FIG. 9. The EPSR estimated hydrogen-hydrogen partial structure factors $[S_{HH}(Q)-1]$ for VHDA, HDA, LDA, ASW, and HGW that are consistent with the measured experimental data. For clarity each function is vertically offset by 0.0, 1.5, 3.0, 4.5, and 6.0 units, respectively.

between the water molecule oxygen sites (O–O), (ii) between the oxygen and hydrogen sites (O–H), and lastly (iii) between the hydrogen sites (H–H). The EPSR derived site-site partial structure factors are shown in Figs. 7–9, for the five ices investigated, and the corresponding pair distribution functions are shown in Figs. 10–12.

An examination of the partial structure factors and pair distribution functions for the five amorphous ices immediately highlights the similarity between LDA, ASW, and HGW. Structural parameters evaluated for ASW and HGW on the intermolecular length scales studied here, <18 Å, corresponding to half the size of the simulation box used during the structure refinement, show these two ice structures to be structurally indistinguishable from LDA.

FIG. 8. The EPSR estimated oxygen-hydrogen partial structure factors $[S_{OH}(Q)-1]$ for VHDA, HDA, LDA, ASW, and HGW that are consistent with the measured experimental data. For clarity each function is vertically offset by 0.0, 2.0, 4.0, 6.0, and 8.0 units, respectively.
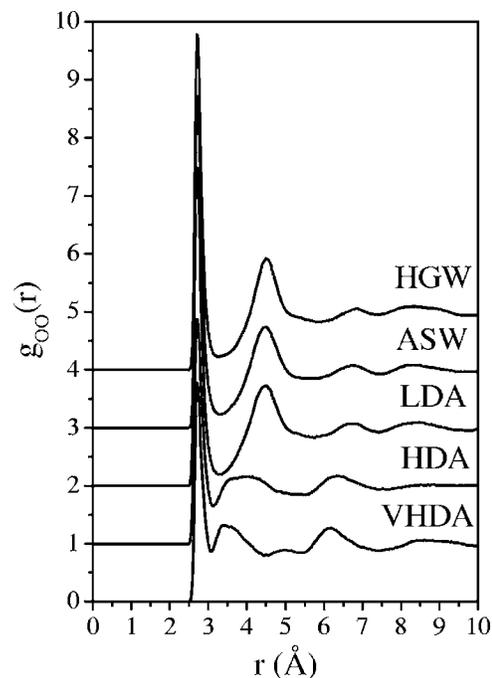

FIG. 10. The EPSR estimated intermolecular oxygen-oxygen pair distribution functions $g_{OO}(r)$ for VHDA, HDA, LDA, ASW, and HGW. For clarity each function is offset by 0.0, 1.0, 2.0, 3.0, and 4.0 units, respectively.
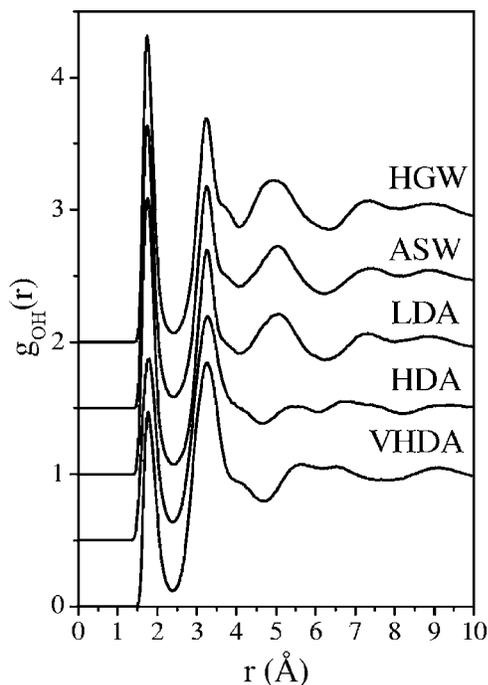
FIG. 11. The EPSR estimated intermolecular oxygen-hydrogen pair distribution functions $g_{OH}(r)$ for VHDA, HDA, LDA, ASW, and HGW. For clarity each function is offset by 0.0, 0.5, 1.0, 1.5, and 2.0 units, respectively.

The pair distribution functions provide us with information on the interatomic distance correlations between the atoms; they can be integrated to give the average number of atoms within a given distance range around an arbitrary atom placed at the origin. This information, presented via the running coordination number $N(r)$, is shown for $g_{OO}(r)$ and $g_{OH}(r)$ in Figs. 13 and 14.

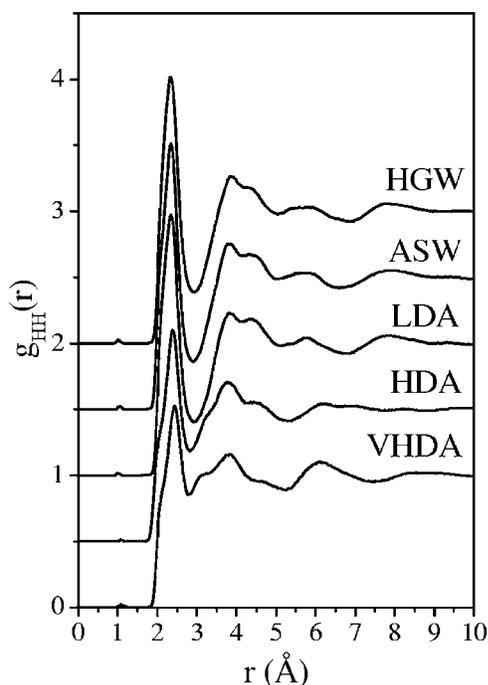FIG. 12. The EPSR estimated intermolecular hydrogen-hydrogen pair distribution functions $g_{HH}(r)$ for VHDA, HDA, LDA, ASW, and HGW. For clarity each function is offset by 0.0, 0.5, 1.0, 1.5, and 2.0 units, respectively.

A first neighbor coordination number analysis of $g_{OO}(r)$ and $N_{OO}(r)$ (Fig. 13) shows that LDA, ASW, and HGW are almost perfectly fourfold coordinated, with each water molecule surrounded on average by four neighboring water molecules in the intermolecular distance range from 2.5 to 3.3 Å. This is consistent with the optimal hydrogen bonding coordination number of two hydrogen atoms H bonded to each water oxygen atom that is shown by the first peak in the distance range from 1.4 to 2.4 Å of $g_{OH}(r)$ and $N_{OH}(r)$ (Fig. 14). The relative positions of the first and second peaks in $g_{OO}(r)$, 2.7(5) and 4.4(5) Å, additionally tell us that the mean O–O–O angle in the LDA network is $\approx 111°$, close to the ideal tetrahedral angle of 109°. We can thus conclude that the short range structures of LDA, ASW, and HGW all relate closely to a hydrogen bonded tetrahedral network of water molecules.

The structures of HDA and VHDA are somewhat more complex. A coordination number analysis for these ices of $g_{OO}(r)$ and $N_{OO}(r)$ in the distance range from 2.5 to 3.1 Å shows (Fig. 13) that each oxygen atom is again immediately coordinated by approximately four neighboring water oxygen atoms. In contrast to LDA, where $N_{OO}(r)$ remains close to this value up to a distance of ≈ 3.4 Å, by this point the oxygen coordination number in HDA rises to ≈ 5 and to a value of ≈ 6 in VHDA. Again $g_{OH}(r)$ and $N_{OH}(r)$ tell us that each water oxygen is hydrogen bonded to two hydrogen atoms in the distance range from 1.4 to 2.4 Å, corresponding to a four-coordinated hydrogen bonded network. These findings are thus consistent with the "interstitial" nonbonded water molecule model first presented in Refs. 9 and 10.

B. Bhatia-Thornton partial structure factors and pair distribution functions

Bhatia and Thornton[30] showed that it was possible to formulate the partial structure factors for a binary system in such a way as to show the correlations between the particle number density N and concentration of atomic species c in the system. These three partial structure factors are termed $S_{NN}(Q)$, $S_{cc}Q$, and $S_{Nc}(Q)$. $S_{NN}(Q)$ reflects the density correlations between the atomic sites regardless of their chemical species, effectively treating all atoms as equal. $S_{cc}(Q)$ in contrast represents the correlations between the differing chemical species and $S_{Nc}(Q)$ the cross correlations. It is worth pointing out here that because to within 1 part in 10^{-7} there are two hydrogen atoms attached to every oxygen atom in water, the concentration-concentration fluctuations must be close to zero at large distance scales ($Q \sim 0$). Hence only the NN Bhatia-Thornton structure factor can show significant positive deviations above zero at small Q.

These partial structure factors are simply related to the previously discussed Faber-Ziman partial structure factors and can be calculated for a water system by the following linear sums:

$$S_{NN}(Q) = c_O^2 S_{OO}(Q) + c_H^2 S_{HH}(Q) + 2c_O c_H S_{OH}(Q),$$

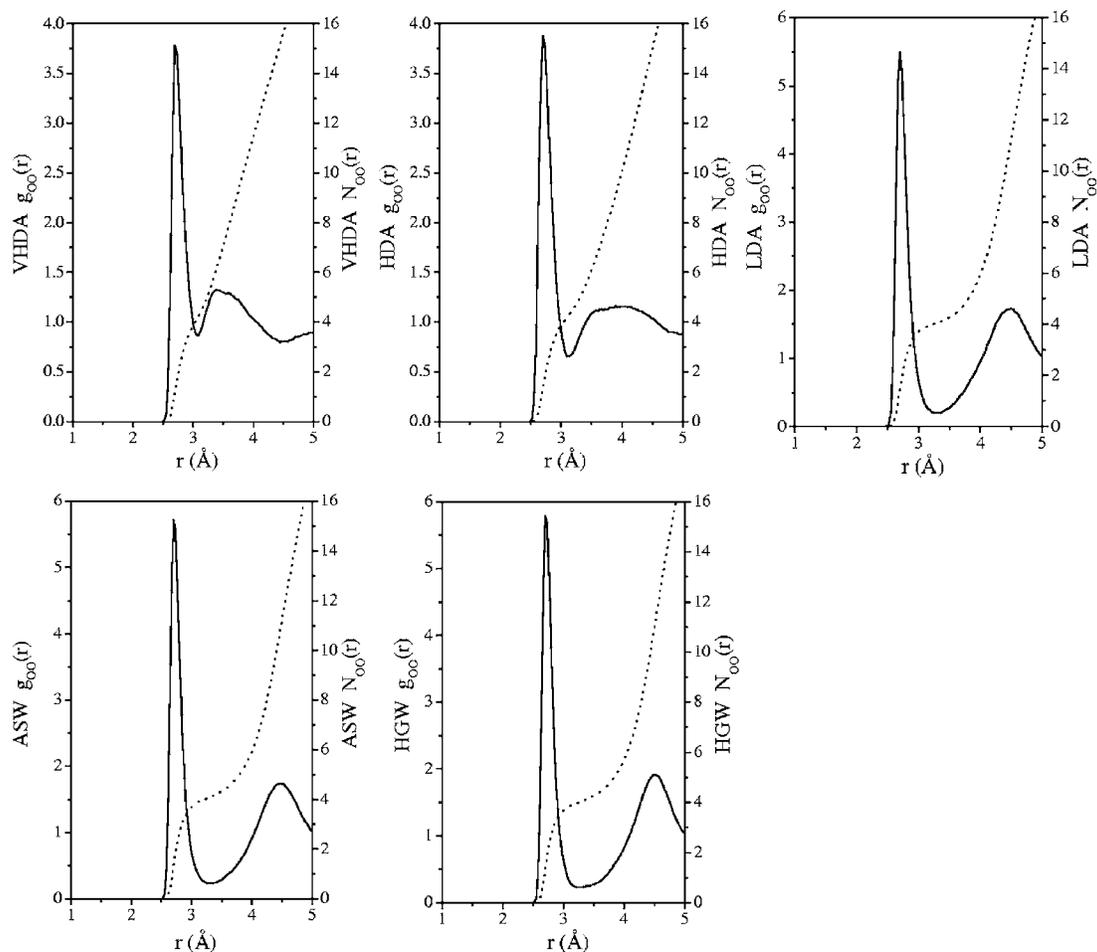$$S_{Nc}(Q) = c_O c_H [c_O (S_{OO}(Q) - S_{OH}(Q)) - c_H (S_{HH}(Q) - S_{OH}(Q))],$$

FIG. 13. Comparison of $g_{OO}(r)$ (solid lines) and $N_{OO}(r)$ (broken lines) for VHDA, HDA, LDA, ASW, and HGW illustrating the relationship between interatomic separation and coordination number of oxygen neighbors around any arbitrarily selected oxygen within the ice structure.

$$S_{cc}(Q) = c_O c_H [1 + c_O c_H (S_{OO}(Q) + S_{HH}(Q) - 2S_{OH}(Q))].$$

$$(5)$$

c_O and c_H are the concentrations of oxygen and hydrogen within the system, here $1/3$ and $2/3$, respectively. Figures 15–17, respectively, show the Bhatia-Thornton $S_{NN}(Q)$, $S_{cc}(Q)$, and $S_{Nc}(Q)$ partial structure factors for VHDA, HDA, LDA, ASW, and HGW.

Strictly speaking the Bhatia-Thornton structure factors are only truly meaningful when considering a binary atomic system. In the case of a monomolecular system such as ice, it is inevitable that every oxygen atom will be coordinated to two hydrogen atoms at a distance of 0.98 Å and these molecules by definition must be distributed throughout the sample volume on all length scales. To take into account the molecular nature of amorphous ices we calculate the intermolecular Bhatia-Thornton partial structure factors and corresponding Bhatia-Thornton partial distribution functions. By removing the intramolecular correlations from these functions the intermolecular correlations between number density and concentration are enhanced. The intermolecular Bhatia-Thornton structure factors are shown in Figs. 18–20 and the corresponding partial distribution functions in Figs. 21–23.

An examination of the Bhatia-Thornton structure factors,

either including the intramolecular terms or in their absence, and comparing them with the total D_2O total structure factors (Fig. 1) for the amorphous ices, allows us to determine the dominant factor that gives rise to the first diffraction peak in the total structure factor. The comparison between the total intramolecular plus intermolecular $S_{NN}(Q)$ structure factor (Figs. 15 and 18) with the pure intermolecular function satisfactorily confirms that the first diffraction peak is solely a function of the intermolecular organization and not the result of a dominant intramolecular correlation length. The peak is known to be associated with the intermediate range order in a system and can arise from either the topology of the atomic or molecular network or from chemical fluctuations within the system. The fact that the first diffraction peak is a characteristic of the $S_{NN}(Q)$ partial structure factor tells us that in the amorphous ice system, the intermediate range order is governed by the network topology and not by fluctuations in the chemical composition. With hindsight this is obvious; as previously stated the system is monomolecular and thus the only means by which intermediate range order can be generated in this system is through the topology of the amorphous network. Stated another way this shows that the structural differences between the different ice structures are not due to chemical fluctuations.

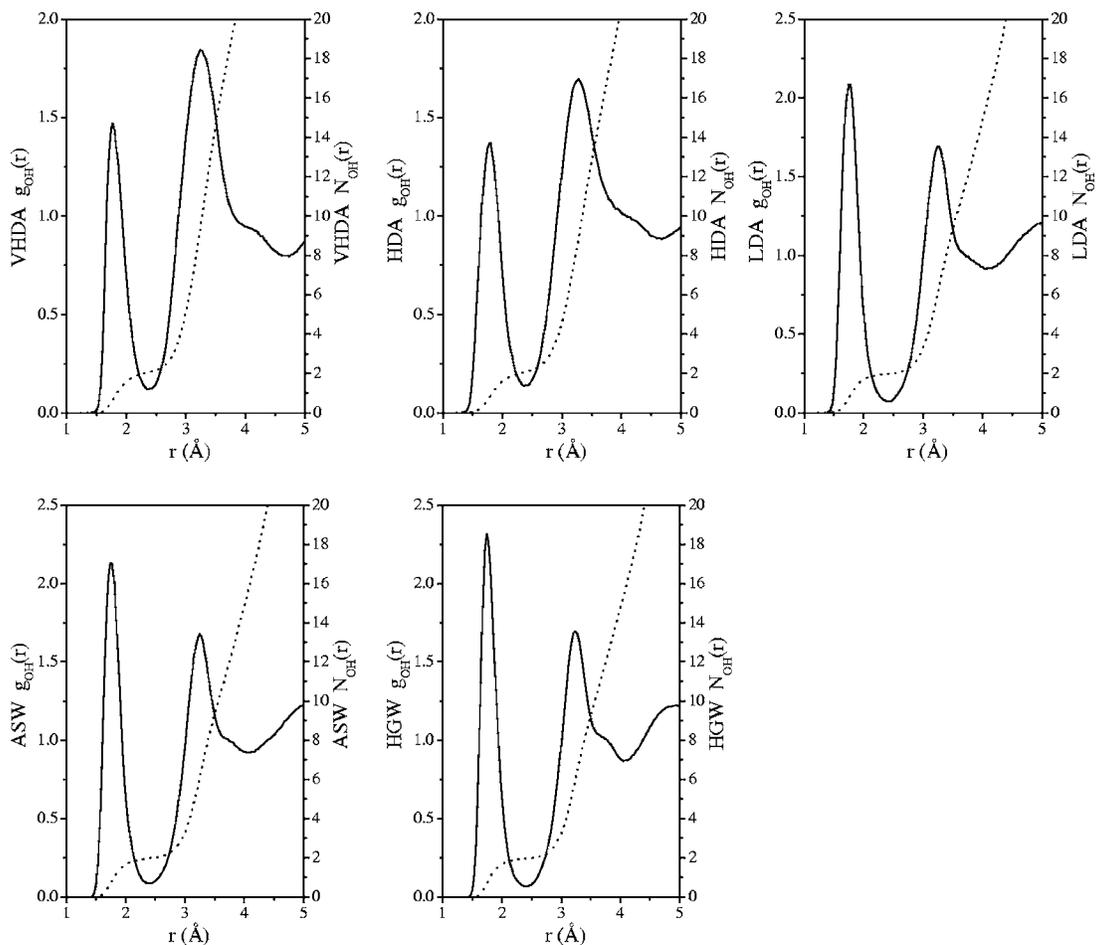A further observation one can make is that the $S_{cc}(Q)$,

FIG. 14. Comparison of $g_{OH}(r)$ (solid lines) and $N_{OH}(r)$ (broken lines) for VHDA, HDA, LDA, ASW, and HGW illustrating the relationship between interatomic separation and coordination number of hydrogen neighbors around any arbitrarily selected oxygen within the ice structure or vice versa.
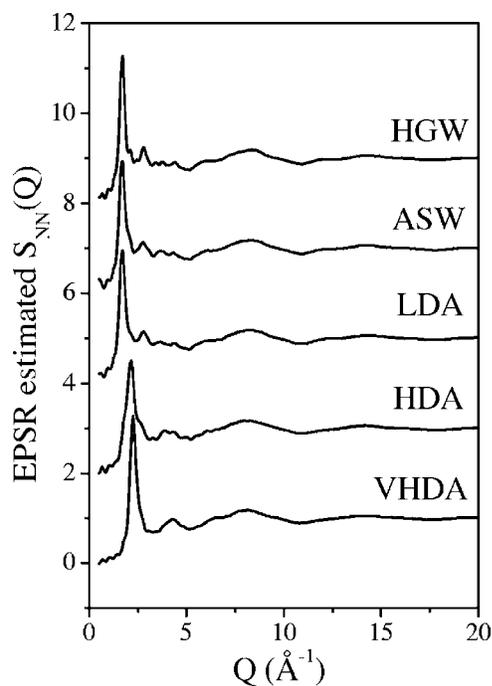

FIG. 15. Bhatia-Thornton number-number partial structure factors, $S_{NN}(Q)$ for VHDA, HDA, LDA, ASW, and HGW. For clarity each function has been offset by 0.0, 2.0, 4.0, 6.0, and 8.0 units, respectively.
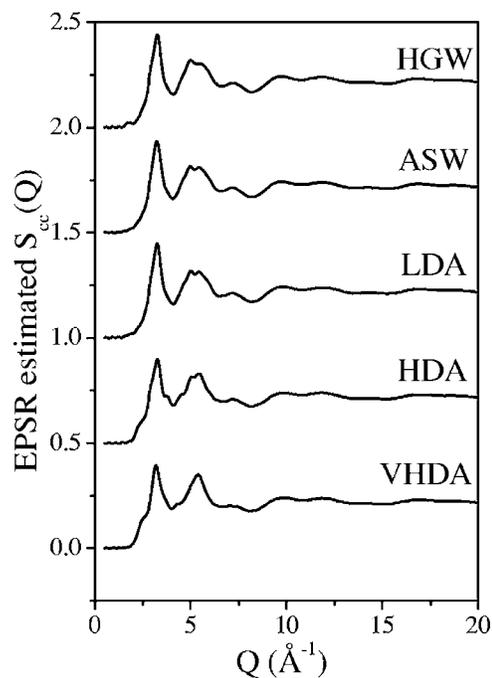
FIG. 16. Bhatia-Thornton concentration-concentration partial structure factors $S_{cc}(Q)$ for VHDA, HDA, LDA, ASW, and HGW. For clarity each function has been offset by 0.0, 0.5, 1.0, 1.5, and 2.0 units, respectively.
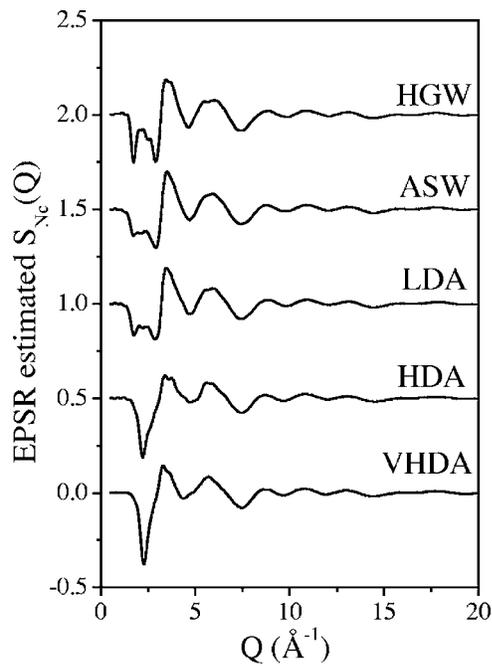
FIG. 17. Bhatia-Thornton number-concentration partial structure factors $S_{Nc}(Q)$ for VHDA, HDA, LDA, ASW, and HGW. For clarity each function has been offset by 0.0, 0.5, 1.0, 1.5, and 2.0 units, respectively.

FIG. 19. Intermolecular Bhatia-Thornton concentration-concentration partial structure factors $S_{cc}(Q)$ for VHDA, HDA, LDA, ASW, and HGW. For clarity each function has been offset by 0.0, 0.5, 1.0, 1.5, and 2.0 units, respectively.

Fig. 16, look remarkably similar to the diffraction data for light water, Fig. 2. This is because the negative neutron scattering length of H compared to the positive scattering length for O means that the net scattering length of this sample is close to zero, so the light water diffraction pattern is dominated by the concentration fluctuations.

Figure 21, $g_{inter,NN}(r)$, allows an interesting comparison of the atomic organization of the network structure, whether the observer is situated on either an oxygen or hydrogen atomic site. In the short distance range $\leqslant \approx 3$ Å, clear oscillations are visible in this function for the low density amorphous ice systems LDA, ASW, and HGW. Such fluctuations are indicative of a well defined local order. In contrast, the short range network connectivity in the high density and very high density ice phases is considerably more homogeneous
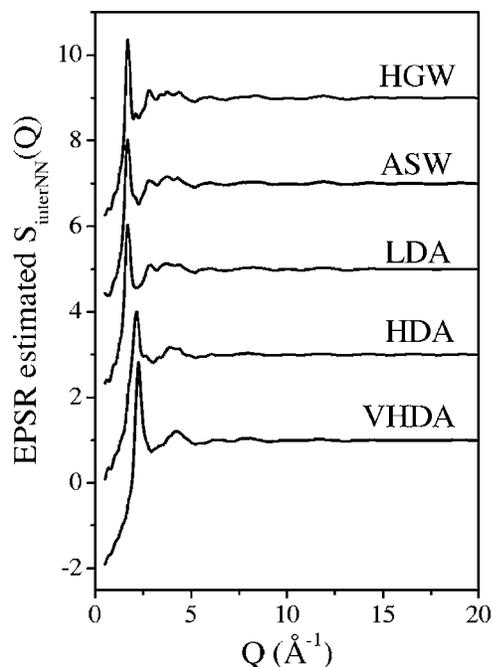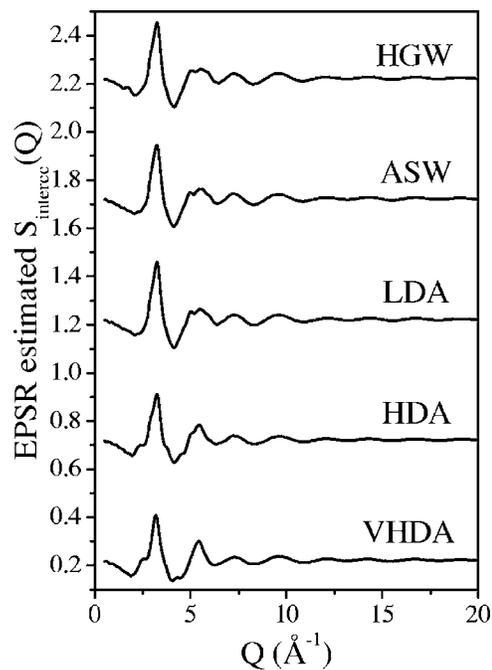

FIG. 18. Intermolecular Bhatia-Thornton number-number partial structure factors $S_{NN}(Q)$ for VHDA, HDA, LDA, ASW, and HGW. For clarity each function has been offset by 0.0, 2.0, 4.0, 6.0, and 8.0 units, respectively.
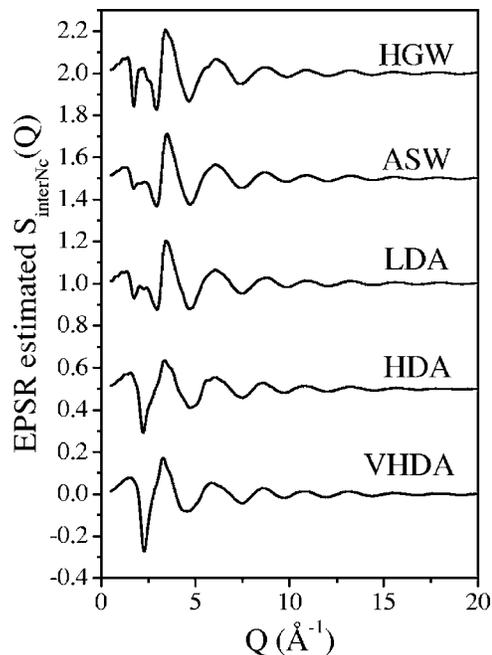

FIG. 20. Intermolecular Bhatia-Thornton number-concentration partial structure factors $S_{Nc}(Q)$ for VHDA, HDA, LDA, ASW, and HGW. For clarity each function has been offset by 0.0, 0.5, 1.0, 1.5, and 2.0 units, respectively.
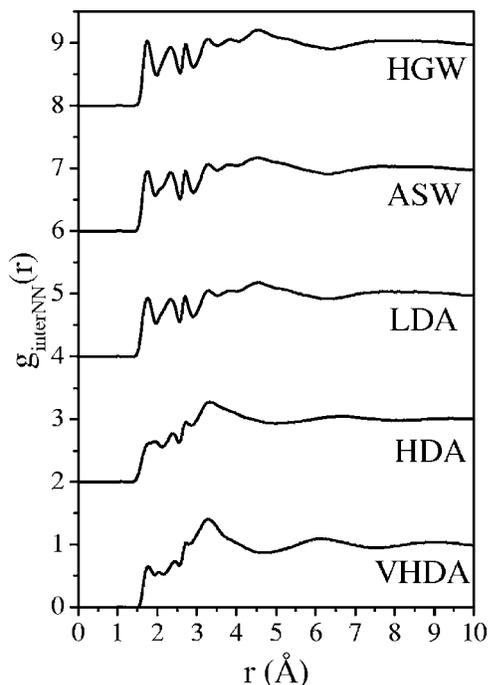
FIG. 21. Intermolecular Bhatia-Thornton number-number partial distribution functions $g_{NN}(Q)$ for VHDA, HDA, LDA, ASW, and HGW. For clarity each function has been offset by 0.0, 2.0, 4.0, 6.0, and 8.0 units, respectively.

FIG. 23. Intermolecular Bhatia-Thornton number-concentration partial distribution functions $g_{Nc}(Q)$ for VHDA, HDA, LDA, ASW, and HGW. For clarity each function has been offset by 0.0, 0.5, 1.0, 1.5, and 2.0 units, respectively.

and the primary topological structural fluctuations appear beyond this distance. These differences thus appear to reflect the distortion of the dominant tetrahedral local structural motifs in the more dense materials but in all the amorphous ice phases topological characteristics are seen to fluctuate up to length scales of at least 10 Å.
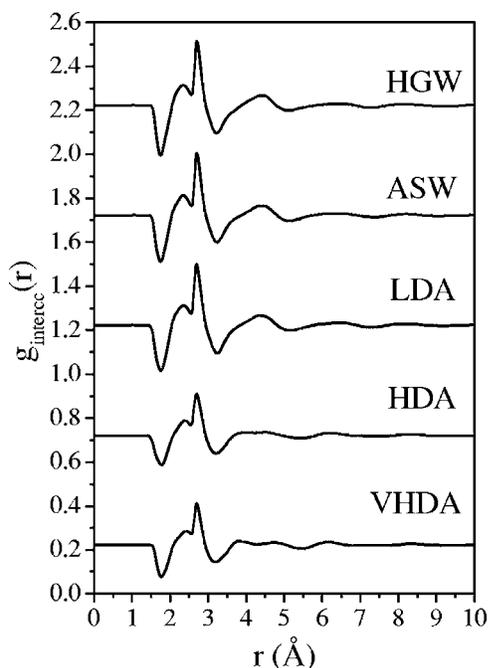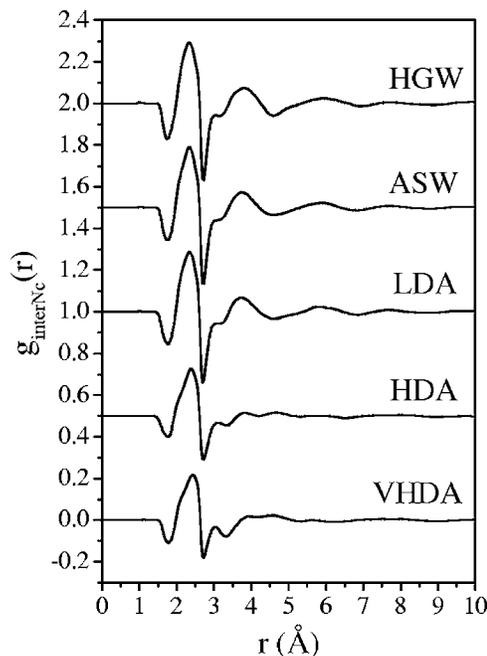

FIG. 22. Intermolecular Bhatia-Thornton concentration-concentration partial distribution functions $g_{cc}(Q)$ for VHDA, HDA, LDA, ASW, and HGW. For clarity each function has been offset by 0.0, 0.5, 1.0, 1.5, and 2.0 units, respectively.

As a next step it is now interesting to compare the features in Fig. 22, $g_{inter,cc}(r)$, with the features seen in the Faber-Ziman pair distribution functions shown in Figs. 10–12 to learn about how the chemical ordering of the hydrogen and oxygen sites is reflected in the local structure. Peaks in $g_{inter,cc}(r)$ reflect correlations between like chemical species as a function of distance, while troughs reflect cross correlations between unlike species. The trough at 1.77 Å relates to the hydrogen bonding interaction between water oxygen atoms and neighboring molecule hydrogen atoms, while the sharp peak at 2.7 Å reflects the strong correlations between the oxygen atoms within the fourfold coordinated network. For completeness it is worth acknowledging that the broad feature in the region between 2.0 and 2.5 Å reflects the range of like species correlations between hydrogen atoms. Compared to the tetrahedral oxygen feature at 2.7 Å, this region reflects the higher level of structural disorder in the hydrogen site correlations by virtue of the enhanced breadth and reduced intensity of this feature. In particular, this enhanced hydrogen site disorder appears to be slightly more marked in the VHDA and HDA phases. What is particularly evident is that, on short length scales <3.1 Å, all the amorphous ice phases are structurally quite similar and demonstrate that the local structure is largely dominated by the intrinsic chemical ordering associated with the water molecule's two donor and two acceptor hydrogen bonding sites. However, beyond this length scale marked differences appear between VHDA, HDA, and LDA/ASW/HGW.

A particular strength of the Bhatia-Thornton formalism is the insight that these partial structure factors can provide into the long wavelength limit fluctuations present in the system, as reflected in the value of the partial structure factors as $Q \rightarrow 0$. In particular, $S_{cc}(0)$ reflects the long range

fluctuations in the composition. Naturally, if the intramolecular terms are included in this function, the $Q \to 0$ limit appears to tend toward a value very close to 0, reflecting the absence of any long-range atom-type fluctuations and consistent with the known monomolecular composition of the sample. In contrast $S_{inter,cc}(0)$ appears to tend towards a value very close to the product of $c_O c_H = 0.2222$ (Fig. 19), which would indicate random mixing of the two components in terms of the intermolecular interactions. This reflects the isotropic nature of the amorphous material and the largely featureless form of $g_{inter,cc}(r)$ beyond the first molecular coordination shell (Fig. 22). Naturally, the extent of this picture is limited by the minimum Q value of 0.5 Å^{-1} investigated in this work, and can only therefore attest to fluctuations on length scales $\leq \approx 10$ Å. A recent neutron diffraction study of the small angle scattering of the amorphous ices[31] has highlighted a low Q contribution in the structure factor of HDA. This signal becomes apparent at Q values below 0.5 Å^{-1}, investigated in the present work, and continues to rise below the minimum Q value of 0.3 Å^{-1} investigated in Ref. 31. This small angle scattering signal corresponds to structural texture on length scales greater than 20 Å in the HDA system that cannot be directly addressed by the data presented here. One possible explanation for this signal is the development of mesoscale texture in the structure of HDA samples during their formation due to the need to accommodate stresses within the water network. The absence of the small angle signal in the VHDA and LDA systems would then suggest that this stress induced structure can effectively be annealed out during their formation as both these glasses can be produced by thermal treatment of HDA either at high (VHDA) or ambient pressure (LDA).

As the long wavelength limit of $S_{cc}(Q)$ tends to 0 (Fig. 16), the corresponding limit for $S_{NN}(Q)$ is dominated in a system under thermodynamic equilibrium by the isothermal compressibility limit. For water at ambient conditions this limit is ~0.18 per atom. This limit is not well defined in a nonequilibrium structure such as a glass; the data available here to the Q_{min} of 0.5 Å^{-1} point towards typical waterlike behavior, with a very small value for $S_{NN}(Q)$ as Q goes to zero (Fig. 15).

C. The total x-ray structure factors

For completeness we calculate the structure factors for the amorphous ices as they would be expected to be measured by x-ray diffraction. As x-ray sources are far more accessible than neutron sources and often provide the only practical means to rapidly verify the structure of an ice sample produced in a laboratory, x-ray structure factors consistent with the neutron scattering data can be useful in future work on the amorphous ice system. Figure 24 thus shows the x-ray structure factor that would be consistent with the three isotopically distinct neutron scattering data sets collected for each of the amorphous ice samples. By and large this is very similar to the Faber-Ziman oxygen-oxygen partial structure factor as x rays are weighted towards the regions of higher electron density, though at low Q, the hydrogen correlations become significant. For LDA and HDA,
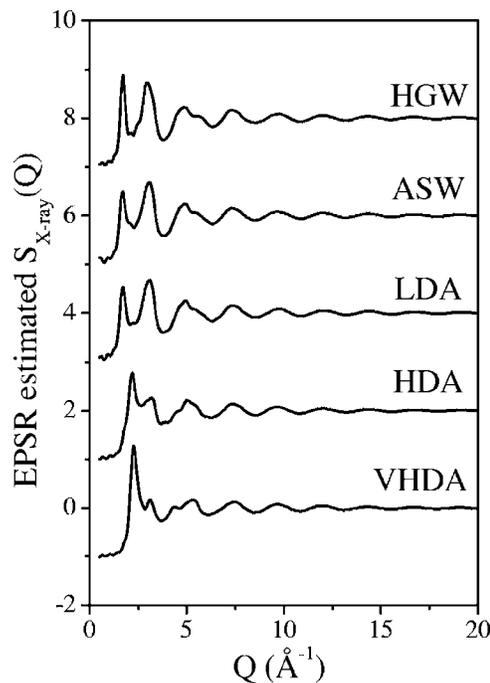

FIG. 24. The EPSR estimated x-ray total structure factors $[S_{x\text{-ray}}(Q) - 1]$ for VHDA, HDA, LDA, ASW, and HGW, that would be consistent with the measured experimental neutron scattering data. The x-ray weighting factors were calculated using the independent atom form factor approximation. For clarity each function is vertically offset by 0.0, 2.0, 4.0, 6.0, and 8.0 units, respectively.

these simulated x-ray structure factors, based on models derived from the neutron data, are highly comparable to those available for comparison in the literature.[14,32]

D. The structure of HDA

Several recent studies have investigated the transformation of VHDA and HDA to LDA and vice versa.[31–35] These studies have suggested that many distinct amorphous states can exist. The fact that the density of HDA is intermediate between VHDA and LDA allows us to test whether HDA could be formed from a mixture of the two limiting cases. Loerting *et al.*[34,35] have recently shown that there is a stepwise character to the formation of VHDA from LDA, apparently indicating that HDA is indeed a distinct structural state, while the annealing studies of Tulk *et al.*[32] and Koza *et al.*[33] indicate that many distinct structural states between HDA and LDA can be accessed by annealing the dense ice system and calling into question whether HDA should, in fact, be considered only one of the complex intermediate structures that are expected to be produced in annealing VHDA and following its transformation to LDA. To investigate the relationship between the recovered HDA sample studied here and the recovered VHDA and LDA samples, we have therefore performed a simple two component analysis of $g_{OO}(r)$. Figure 25 shows the best fit linear combinations obtained either by fitting the height of the first peak in $g_{OO}(r)$ or by fitting the intermediate density of the HDA system. It is clear from this figure that the sample of HDA studied here is structurally distinct and not directly related by a simple linear combination of the two other amorphous states.
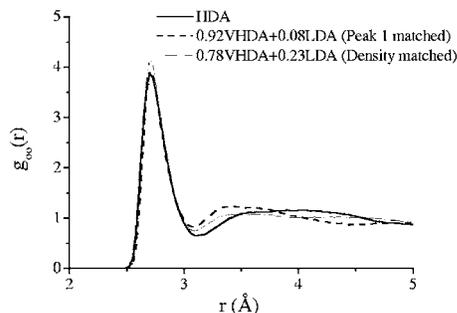
FIG. 25. Two component fits of VHDA and LDA to HDA using $g_{OO}(r)$ to distinguish between the structures of the mixture models and the experimentally measured HDA sample.

VI. CONCLUSIONS

The Faber-Ziman partial pair distribution functions demonstrate clearly that the atomic level structures of ASW and HGW are the same and indistinguishable from that of LDA. There are also no significant structural differences between these three systems on length scales up to about 10 Å. Within the precision of these measurements all three of these low density ices are essentially fourfold coordinated hydrogen bonded structures, with each water molecule donating and accepting two hydrogen bonds. All three structures do indeed resemble closely a tetrahedral random network of hydrogen bonded water molecules.

The reanalysis of the data for HDA and VHDA confirms that these structures are more complex. Interestingly, in the first neighbor region up to about 3.1 Å from a central water oxygen, these networks are still on average tetrahedrally coordinated, with each oxygen site donating and accepting two hydrogen bonds to neighboring molecules. Just beyond this region, however, the oxygen coordination number rises to ≈ 5 for HDA and ≈ 6 for VHDA, consistent with the "interstitial" concept proposed earlier.[9,10] We emphasize that these interstitials themselves are also on average fully hydrogen bonded water molecules, so there must be a considerable degree of hydrogen bond bending in these materials compared to LDA.

The Bhatia-Thornton analysis uncovers some further interesting aspects of these structures. The first diffraction peak in all five structures is confirmed to be solely a function of the intermolecular organization, and is not the result of a dominant intramolecular correlation length (or of "chemical ordering"). More interestingly, the short range network connectivity in the two higher density systems is more homogeneous than in the lower density LDA/ASW/HGW structure, and is a consequence of a greater distortion of the dominant local tetrahedral structural motif in the higher density systems. Presumably related to this observation, there is a higher degree of hydrogen site disorder in HDA and VHDA than in LDA/ASW/HGW. This analysis also shows clearly that on the short length scales <3.1 Å, all these amorphous ices are structurally quite similar, being dominated by the intrinsic chemical ordering forced by the water molecule's ability to simultaneously donate and accept two hydrogen bonds. It is beyond this length scale that the marked differences are found between VHDA and HDA on the one hand, and LDA/ASW/HGW on the other.

The Bhatia-Thornton analysis throws interesting light on the long wavelength fluctuations in these systems. Within the limits of the data (the Q_{min} of 0.5 Å^{-1} limits the length scales probed to $\leqslant \approx 10$ Å), the way in which the structure factors for all these structures approach the $Q \rightarrow 0$ limit is consistent with a random mixing in terms of intermolecular interactions. Furthermore, the results are consistent with waterlike compressibility behavior.

Finally, the finding that the sample of HDA studied here is structurally distinct and not directly related to a simple linear combination of VHDA and LDA emphasizes that on the length scales of this structural study, up to distances of ≈ 10 Å, these materials do, in fact, have independent structural forms. The Bhatia-Thornton analysis allows us to associate the differences between these three structures predominantly with variations in the local topology and not to local chemical ordering. The chemical ordering, as stated earlier, is similar for all three amorphous systems, though with decreasing degrees of short range hydrogen site disorder as the structures are sequentially compared from VHDA to HDA to LDA.

[1] E. F. Burton and W. F. Oliver, Proc. R. Soc. London, Ser. A **153**, 166 (1935).
[2] V. F. Petrenko and R. W. Whitworth, *Physics of Ice* (Oxford University Press, Oxford, 1999).
[3] E. Mayer and R. Pletzer, Nature (London) **319**, 298 (1986).
[4] E. Mayer and P. Brüggeller, Nature (London) **298**, 715 (1982).
[5] E. Mayer, J. Appl. Phys. **58**, 663 (1985).
[6] O. Mishima, L. D. Calvert, and E. Whalley, Nature (London) **310**, 393 (1984).
[7] O. Mishima, L. D. Calvert, and E. Whalley, Nature (London) **314**, 76 (1985).
[8] T. Loerting, C. Salzmann, I. Kohl, E. Mayer, and A. Hallbrucker, Phys. Chem. Chem. Phys. **3**, 5355 (2001).
[9] J. L. Finney, D. T. Bowron, A. K. Soper, T. Loerting, E. Mayer, and A. Hallbrucker, Phys. Rev. Lett. **89**, 205503 (2002).
[10] J. L. Finney, A. Hallbrucker, I. Kohl, A. K. Soper, and D. T. Bowron, Phys. Rev. Lett. **88**, 225503 (2002).
[11] M. R. Chowdhury, J. C. Dore, and J. T. Wenzel, J. Non-Cryst. Solids **53**, 247 (1982).
[12] J. C. Dore, J. Mol. Struct. **237**, 221 (1990).
[13] A. Hallbrücker, E. Mayer, L. P. O'Mard, J. C. Dore, and P. Chieux, Phys. Lett. A **159**, 406 (1991).
[14] A. Bizid, L. Bosio, A. Defrain, and M. Oumezzine, J. Chem. Phys. **87**, 2225 (1987).
[15] M.-C. Bellissent-Funel, J. Teixeira, and L. Bosio, J. Chem. Phys. **87**, 2231 (1987).
[16] M.-C. Bellissent-Funel, L. Bosio, A. Hallbrucker, E. Mayer, and R. Sridi-Dorbez, J. Chem. Phys. **97**, 1282 (1992).
[17] A. K. Soper, Phys. Rev. B **72**, 104204 (2005).
[18] D. A. Keen, J. Appl. Crystallogr. **34**, 172 (2001).
[19] J. L. Finney and A. K. Soper, Chem. Soc. Rev. **23**, 1 (1994).
[20] V. F. Sears, Neutron News **3**, 29 (1992).
[21] A. Hallbrucker and E. Mayer, J. Chem. Soc., Faraday Trans. **86**, 3785 (1990).

[22] I. Kohl, L. Bachmann, A. Hallbrucker, E. Mayer, and T. Loerting, Phys. Chem. Chem. Phys. **7**, 3210 (2005).

[23] P. G. Debenedetti, J. Phys.: Condens. Matter **15**, R1669 (2003).

[24] A. K. Soper (private communication).

[25] A. C. Howells, W. S. Howells, and A. K. Soper, ATLAS: A suite of programs for the analysis of time-of-flight neutron diffraction data from liquid and amorphous samples, 1990 IOP Conf. Series 107 193–211.

[26] A. K. Soper and A. Luzar, J. Chem. Phys. **97**, 1320 (1992).

[27] A. K. Soper, Chem. Phys. **202**, 298 (1996).

[28] A. K. Soper, Mol. Phys. **99**, 1503 (2001).

[29] H. J. C. Berendsen, J. R. Grigera, and T. P. Straatsma, J. Phys. Chem. **91**, 6269 (1987).

[30] A. B. Bhatia and D. E. Thornton, Phys. Rev. B **2**, 3004 (1970).

[31] M. M. Koza, B. Geil, K. Winkel, C. Köhler, F. Czeschka, M. Scheuermann, H. Schober, and T. Hansen, Phys. Rev. Lett. **94**, 125506 (2006).

[32] C. A. Tulk, C. J. Benmore, J. Urquidi, D. D. Klug, J. Neuefeind, B. Tomberli, and P. A. Egelstaff, Science **297**, 1320 (2002).

[33] M. M. Koza, H. Schober, H. E. Fischer, T. Hansen, and F. Fujara, J. Phys.: Condens. Matter **15**, 321 (2003).

[34] T. Loerting, C. G. Salzmann, K. Winkel, and E. Mayer, Phys. Chem. Chem. Phys. **8**, 2810 (2006).

[35] T. Loerting, W. Schustereder, K. Winkel, C. G. Salzmann, I. Kohl, and E. Mayer, Phys. Rev. Lett. **96**, 025702 (2006).